Monthly Notices
of the
ROYAL ASTRONOMICAL SOCIETY

Mon. Not. R. Astron. Soc. **414,** 3036–3043 (2011) doi:10.1111/j.1365-2966.2011.18604.x

Surviving infant mortality in the hierarchical merging scenario

R. Smith,[1]⋆ M. Fellhauer,[1] S. Goodwin[2] and P. Assmann[1]

[1]*Departamento de Astronomia, Universidad de Concepcion, Casilla 160-C, Concepcion, Chile*
[2]*Department of Physics and Astronomy, University of Sheffield, Hicks Building, Hounsfield Road, Sheffield S3 7RH*

Accepted 2011 February 24. Received 2011 February 23; in original form 2011 January 27

ABSTRACT

We examine the effects of gas expulsion on initially substructured and out-of-equilibrium star clusters. We perform *N*-body simulations of the evolution of star clusters in a static background potential before removing that potential to model gas expulsion. We find that the initial star formation efficiency is not a good measure of the survivability of star clusters. This is because the stellar distribution can change significantly, causing a large change in the relative importance of the stellar and gas potentials. We find that the initial stellar distribution and velocity dispersion are far more important parameters than the initial star formation efficiency and that clusters with very low star formation efficiencies can survive gas expulsion. We suggest that it is variations in cluster initial conditions rather than in their star formation efficiencies that cause some clusters to be destroyed while a few survive.

Key words: methods: numerical – stars: formation – galaxies: star clusters: general.

1 INTRODUCTION

Many, perhaps the vast majority of, stars form in a clustered (Bressert et al. 2010) and dense (Lada & Lada 2003) environment However, after only 10–20 Myr the vast majority of stars are dispersed into the low density environment of the field (Lada & Lada 2003). The destruction of most of these early dense clusters has been termed 'infant mortality'.

Perhaps the best candidate for the mechanism behind infant mortality is primordial gas expulsion. Giant molecular clouds turn only a few per cent to a few tens of per cent of their gas into stars (Lada & Lada 2003) meaning that the potentials of very young embedded clusters are dominated by gas. Feedback from the most massive stars will remove this gas on a time-scale of a few Myr significantly altering the potential of the cluster and potentially leading to its destruction. This process has been studied analytically and with simulations by many authors (e.g. Tutukov 1978; Hills 1980; Mathieu 1983; Elmegreen 1983; Lada, Margulis & Dearborn 1984; Elmegreen & Clemens 1985; Pinto 1987; Verschueren & David 1989; Goodwin 1997a,b, 2009; Geyer & Burkert 2001; Boily & Kroupa 2003a,b; Bastian & Goodwin 2006; Goodwin & Bastian 2006; Baumgardt & Kroupa 2007, hereafter BK07; Parmentier et al. 2008; Chen & Ko 2009).

However, previous work has tended to concentrate on clusters that are both in virial equilibrium (notable exceptions are Lada et al. 1984; Elmegreen & Clemens 1985; Verschueren & David 1989; Goodwin 2009) and structurally simple (usually a Plummer sphere or similar). But recent observational and theoretical results strongly suggest that stars do not form in dynamical equilibrium nor in a smooth distribution (see e.g. Elmegreen & Elmegreen 2001; Allen et al. 2007; Gutermuth et al. 2009; Bressert et al. 2010, and references in all of these papers). This should not be surprising as in the gravoturbulent model of star formation, stars will form in dense gas in filaments and clumps in a turbulent environment (see e.g. Elmegreen & Scalo 2004). This has led to a model of star cluster formation in which a dynamically cool and clumpy initial state collapses and violently relaxes into a dense star cluster (e.g. Allison et al. 2009a, 2010).

Strongly non-equilibrium initial conditions may play a crucial role in the effects of gas expulsion on clusters because the key factor in determining the effects of gas expulsion is not only the depth of the gas potential, but also the dynamical state of the stars *at the onset of gas expulsion* (Verschueren & David 1989; Goodwin 2009). As an extreme example, if 99 per cent of the mass of a cluster is expelled, the cluster will still survive if the stars have almost no velocity dispersion.

We might therefore expect the effects of gas expulsion on a cluster to depend on the following three factors: first, a clumpy and non-symmetrical initial distribution of the stars; secondly, the star formation efficiency (SFE), and so the relative importance of the stellar and gas potentials; and thirdly, the (non-equilibrium) initial conditions of the cluster and the evolution of these initial conditions up until the point of gas expulsion. If clusters are unable to relax fully before gas expulsion, then we might expect them to respond very differently to the loss of the residual gas.

In this paper, we examine the *N*-body evolution of a highly non-equilibrium star cluster in fixed background potentials to model the background gas. The background potential is then removed to simulate the effects of gas expulsion. We describe our initial

⋆E-mail: rsmith@astro-udec.cl

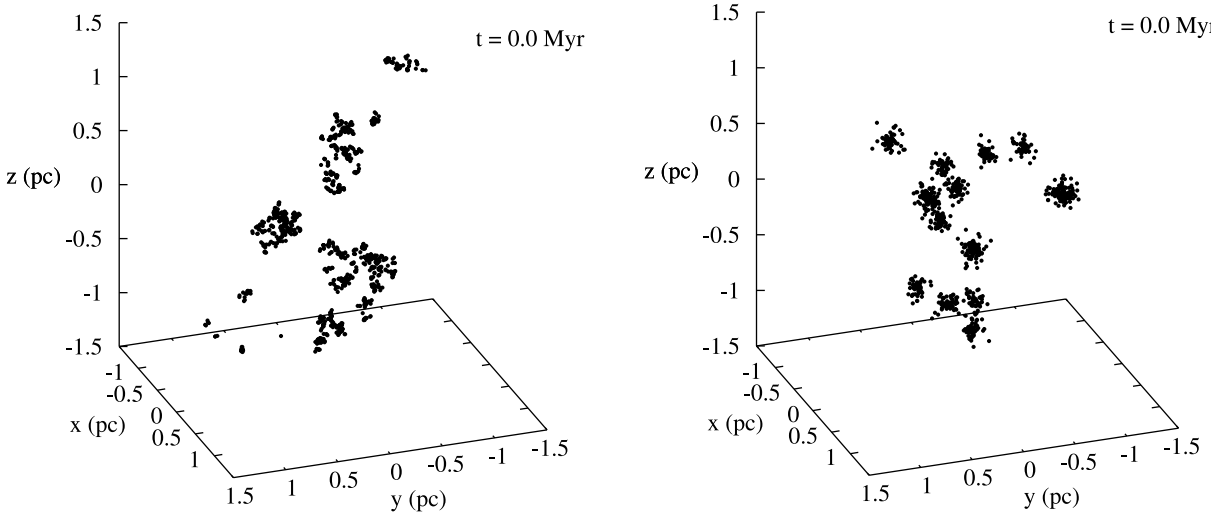

Figure 1. Representative examples of an initial distribution of stars with a fractal morphology (left-hand panel) and a clumpy Plummer morphology (right-hand panel).

conditions in Section 2, our results in Section 3 and then discuss the potential consequences in Section 4 before drawing our conclusions in Section 5.

2 INITIAL CONDITIONS

We perform our *N*-body simulations using the NBODY2 code (Aarseth 2001). NBODY2 is a fast and accurate direct-integration code, optimized for the number of star particles used in this study ($N = 1000$). In our simulations, there are two separate mass distributions which we wish to model: the stars and the background gas potential.

2.1 Stellar distribution

In all cases, we model the stellar distribution as $N = 1000$ particles with equal masses of $0.5\,M_\odot$ resulting in a total stellar mass of $500\,M_\odot$. Every particle has a gravitational softening length of 100 au. We choose softened and equal-mass particles in order to avoid strong 2-body interactions and mass segregation. Allison et al. (2009a, 2010) showed that both of these effects can be extremely important in the violent collapse of cool, clumpy regions; however, we wish to avoid complicating our simulations with these effects as we are interested in the effects of gas expulsion.

We distribute the stars within a radius of 1.5 pc with two different 'clumpy' morphologies: 'fractal' and 'clumpy Plummer'. Representative snapshots of the initial conditions of a fractal and clumpy Plummer distribution can be seen in the left-hand and right-hand panels, respectively, of Fig. 1.

Fractal clusters are produced using the box fractal technique described by Goodwin & Whitworth (2004), also used by Allison et al. (2009b, 2010). In this paper, we use a fractal dimension $D = 1.6$ which corresponds to a highly clumpy initial distribution (see Fig. 1).

In clumpy Plummers, each sub-clump is modelled as an individual Plummer sphere. The total stellar mass of $500\,M_\odot$ is distributed into 16 sub-clumps of approximately equal mass. Each sub-clump contains 31.0–$31.5\,M_\odot$ formed from 62–63 particles. The position of individual sub-clumps within the model star-forming region follows the gas potential (see below).

2.2 Gas distribution

The gas within the star-forming region is modelled as a static Plummer potential with a mass M_g and scale-radius r_g.

The scale-radius is set to be $r_g = 1$ or 1.5 pc. As the stars have a maximum radius of 1.5 pc this means that for $r_g = 1.5$ pc, the gas distribution seen by the stars is roughly uniform.

The relative masses of the gas potential within 1.5 pc and the stars set the *true* SFE (ϵ), that is the fraction of the initial cloud mass converted into stars. The mass of the gas potential is varied to obtain true SFEs of 20, 30 and 40 per cent ($M_g = 2000$, 1167 and $750\,M_\odot$).

Note that a true SFE of 20 or 30 per cent will fail to produce a bound star cluster after instantaneous gas expulsion if the gas and stars are initially virialized (see e.g. BK07).

We emphasize that the gas potential does not follow the initial stellar distribution nor does it react to changes in the stellar distribution as it evolves (it is not live). These are obviously extreme simplifications, but as we will discuss later we feel that we capture the essence of the basic physics using such a simple model.

2.3 Dynamical state of the stars

The virial ratio $Q = T/|\Omega|$ is the ratio of the kinetic , T, to potential energy, Ω, of the system. We set the initial velocity dispersion of the stars relative to the total potential (gas and stars) to set initial stellar virial ratios between zero (cold), 0.5 (virial equilibrium) and 0.9 (supervirial, but bound).

For initial virial ratios $Q < 0.5$, the system will tend to collapse, and for $Q > 0.5$ the system will tend to expand. However, even for $Q = 0.5$, although the system is in virial equilibrium, the clumpy initial conditions mean that it is *not* in dynamical equilibrium.

2.4 Gas expulsion

Although young star clusters form embedded within the molecular gas from which they formed, few star clusters over ∼5 Myr old remain associated with their gas (Proszkow & Adams 2009). This is likely as a result of a number of mechanisms including radiative feedback from massive stars, stellar winds from young stars

Table 1. The initial conditions' parameter sets. Parameters are loosely divided into quantities governing the total region (upper), the stellar component (middle) and the gas component (lower). Parameters that are marked with a '*' symbol are parameters that we adjust between simulations.

Total mass, $M_{\rm tot}$	1250–2500 $M_\odot$*
Outer radius	1.5 pc
SFE, ϵ	20–40 per cent*
Total stellar mass, $M_{\rm star}$	500 $M_\odot$
Particle number, N	1000
Particle mass, $m_{\rm part}$	0.5 $M_\odot$
Stellar morphology	Fractal or Plummer*
Initial virial ratio, $Q_{\rm i}$	0.0–1.0*
Total gas mass, $M_{\rm g}$	750–2000 $M_\odot$*
Gas Plummer scale-radius, $r_{\rm g}$	1.0 or 1.5 pc*
Crossing time, $\tau_{\rm cr}$	1.4/2.0 Myr ($r_{\rm g} = 1.0/1.5$ pc)

and eventually the onset of the first supernova. The time at which gas removal begins to occur, and the duration of the gas removal process is uncertain, and dependent on the particular gas removal mechanism in operation.

To simulate gas expulsion, we instantaneously remove the external gas potential after 3 Myr. This is approximately mid-way between the times at which gas removal from stellar winds and supernova feedback might be expected to occur for star clusters containing ∼1000 stars. Instantaneous gas removal is the most extreme form of gas removal as the stars have no chance to readjust to the change in the potential (e.g. Goodwin 1997a; BK07).

2.5 Ensembles

It should be noted that both the clumpy Plummer and the fractal clusters can vary considerably in appearance depending on the random realization used, and the subsequent evolution is highly stochastic (see Allison et al. 2010). We therefore conduct a minimum of five random realizations of each parameter set.

2.6 Summary

We set up clumpy 500-$M_\odot$ star clusters with $N = 1000$ equal-mass particles within a static background gas potential. The dynamical state of the stars varies from very cold to almost unbound. The stars dynamically evolve within the gas potential before its instantaneous removal after 3 Myr. We measure the final properties of each star cluster an additional 3 Myr after gas expulsion. A summary of the key parameters is provided in Table 1.

3 RESULTS

We will first discuss the evolution and relaxation of the stellar distribution in the gas potential before addressing the response of the stars to gas expulsion.

3.1 Embedded phase

In all simulations, we evolve our stellar initial conditions for 3 Myr in the gas potential. In Fig. 2, we present an example of the evolution of an initially fractal stellar distribution with an initial virial ratio of 0.33 in a gas potential of a scale-radius of 1 pc. The initial true SFE of this system is $\epsilon = 20$ per cent.

Clumpy stellar substructure interacts resulting in clump merging and stellar scattering from the clumps (somewhat suppressed in these simulations due to the softening). As a result, substructure is significantly erased on approximately one to two crossing times of the region. For example, the crossing time of the region presented in Fig. 2 is 1.4 Myr. By 3 Myr (bottom-right panel) over two crossing times have elapsed, and the remaining stellar distribution has lost most of its substructure. Similar behaviour is seen in the simulations of Goodwin & Whitworth (2004) and Allison et al. (2009a, 2010). However, they do not include a model for the gas component of the region in their simulations. By including a gas potential in our simulations, the crossing time of the region is shortened. However, the picture of the evolution from clumpy substructure to an almost smooth distribution of stars, on time-scales of approximately one to two crossing times of the region, is unsurprisingly unchanged by the presence of the gas.

Importantly, the relaxation and smoothing of the stellar distribution have resulting in it shrinking significantly (see also Allison et al. 2009a, 2010). It is clear from Fig. 2 that the central regions of the cluster now contain a greater number of stars than what they did initially. This means that (because the gas potential is static) that the stars are a more significant contributor to the central potential than initially – the *effective SFE* has increased (Verschueren & David 1989; Goodwin 2009) and, in this case, the cluster should be more able to survive gas expulsion.

In order to quantify the effects of collapse (or expansion) and the change of the effective SFE, we define the *local stellar fraction* (LSF) of the star-forming region:

$$\mathrm{LSF} = \frac{M_\star(r < r_{\rm h})}{M_\star(r < r_{\rm h}) + M_{\rm gas}(r < r_{\rm h})}, \quad (1)$$

where $r_{\rm h}$ is the radius from the centre of the region containing half the total mass of *stars* and $M_\star$ and $M_{\rm gas}$ are the masses of stars and gas, respectively, measured within $r_{\rm h}$. Therefore, the LSF is a measure of the current effective SFE.

In any non-equilibrium system, the half-mass radius of the stars will change with time. Fig. 3 shows a projection of the stellar distributions of an initially clumpy Plummer model within an $r_{\rm g} = 1$ pc, $M_{\rm g} = 2000\,M_\odot$ gas potential. Initially, the stars have an initial virial ratio of 0.35 and a half-mass radius $r_{\rm h} = 0.78$ pc. LSF = 0.23, close to the initial true SFE of $\epsilon = 0.2$ (left-hand panel). However, at 3 Myr the stellar half-mass radius has fallen to $r_{\rm h} \sim 0.55$ pc and the LSF is 0.73 (right-hand panel) – almost double the initial value.

In Fig. 4, we plot the LSF-measured moments before gas expulsion versus the initial virial ratio of the stars $Q_{\rm i}$. Unsurprisingly, stellar distributions with a low initial virial ratio form clusters with high LSFs. What is slightly surprising is that high-$Q_{\rm i}$ (warm) clusters do not have significantly lower LSFs than their initial true SFE. This is because the gas potential dominates and even almost unbound clusters only expand by a factor of less than 2 in their half-mass radii (some stars are lost, but the half-mass radii do not change by very significant factors). However, there is considerable scatter in the figure. The values with error bars connected by a solid line in Fig. 4 represent the mean values with the standard deviation of this scatter in LSF (for $\epsilon = 0.2$ simulations) measured in 0.1 wide bins of $Q_{\rm i}$. We show a representative histogram for the $Q_{\rm i} = 0.3$–0.4 bin in Fig. 5. On top of our five random realizations of each point of our parameter space, we conduct an additional 60 Plummer and

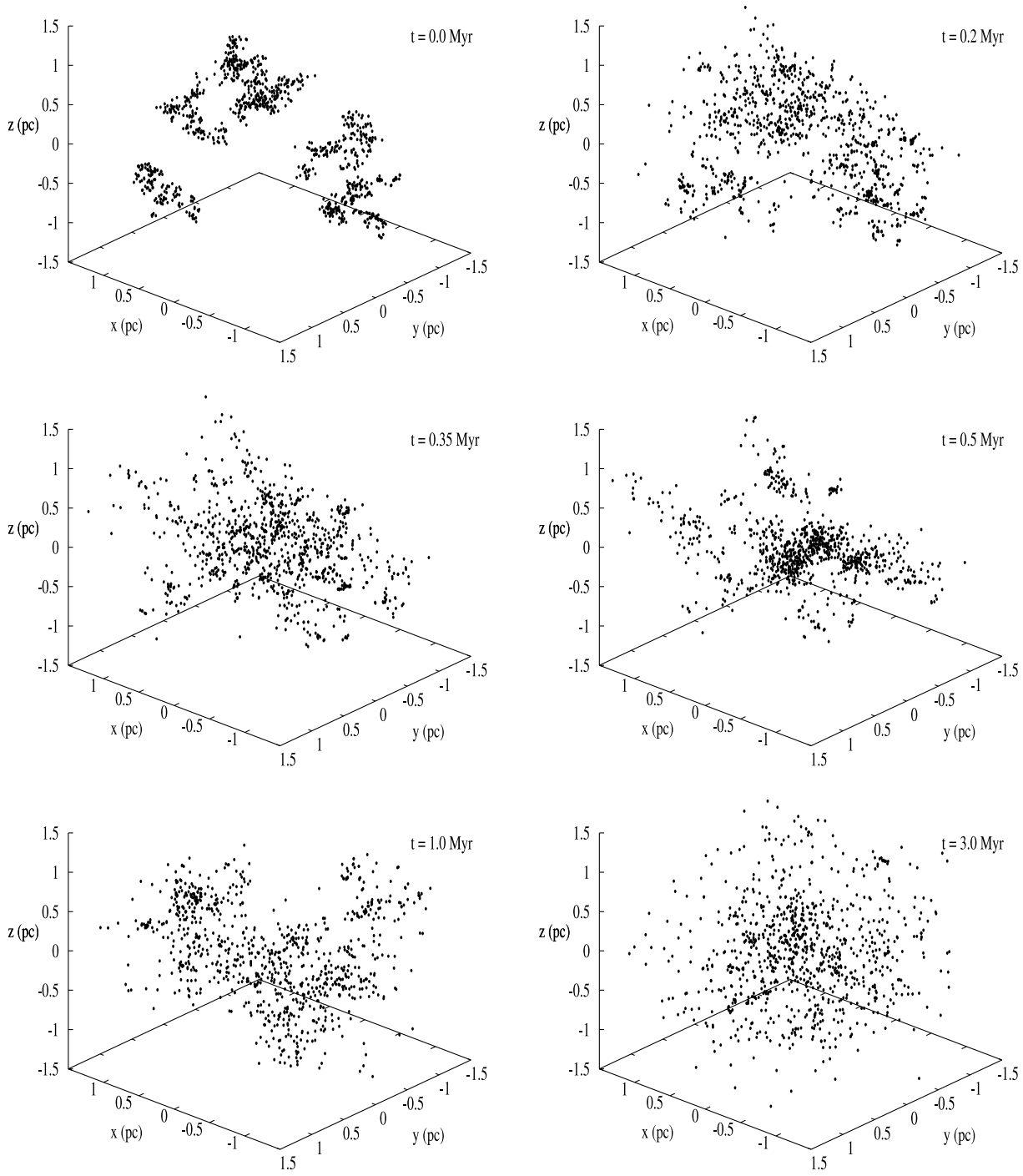

Figure 2. The evolution of an initially fractal ($D = 1.6$) stellar distribution in an $r_g = 1$ pc, $M_g = 2000\,M_\odot$ gas potential. The initial virial ratio of the stellar distribution is 0.33. The time of each snapshot is indicated in the top-right corner of each panel.

70 fractal morphology simulations so as to ensure a minimum of 20 simulations in each Q_i bin to avoid low number statistics. The scatter is higher for stellar distributions with low initial virial ratios. This scatter reflects the stochastic nature of cluster evolution from clumpy initial conditions (see Allison et al. 2010).

We find no evidence for any dependency in the position or scatter of the trend on initial stellar morphology (clumpy Plummer or fractal) or gas concentration (uniform or concentrated). There is a trend in that clusters with higher true SFEs have higher LSFs reflecting their initially higher SFEs (open boxes and triangles in Fig. 4).

As well as the LSF, the virial ratio of the stars at the onset of gas expulsion is also important. In particular, the velocity dispersion of the stars is crucial, with sub-virial clusters being much more able to survive gas expulsion (Goodwin 2009). Therefore, we measure the stellar virial ratio just before gas expulsion Q_{pe}.

Fig. 6 shows the initial and pre-expulsion virial ratios for all our clusters. As would be expected, our clusters have attempted to reach equilibrium (by erasing substructure and collapsing/expanding). In all cases, the clusters have reached an *approximate* virial equilibrium of $Q_{pe} \sim 0.5$. However, it is crucial to note that these are

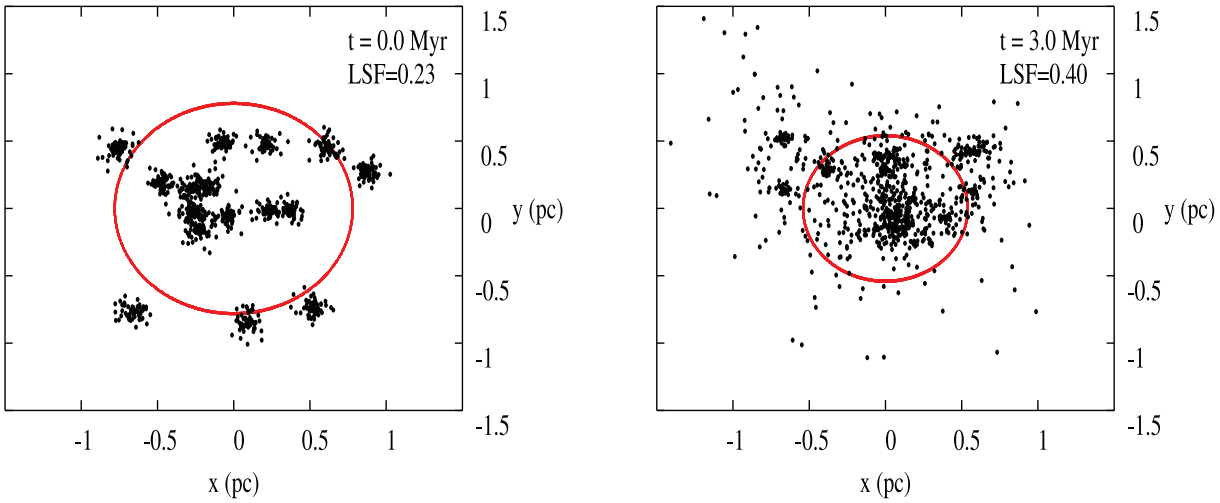

Figure 3. An x–y projection of the initial (left-hand panel) and final (right-hand panel) stellar distributions of an initially clumpy Plummer morphology stellar distribution, evolved for 3 Myr in an $r_g = 1$ pc, $M_g = 2000\,M_\odot$ gas potential. The initial virial ratio of the stellar distribution is 0.35. The time of snapshot and LSF at that instant are indicated in the top-right corner of each panel. The dotted (red) circle marks the stellar half-mass radius, directly used to calculate the LSF. In this case, the LSF almost doubles from 0.23 (left-hand panel) to 0.40 (right-hand panel) over the duration of the embedded phase.

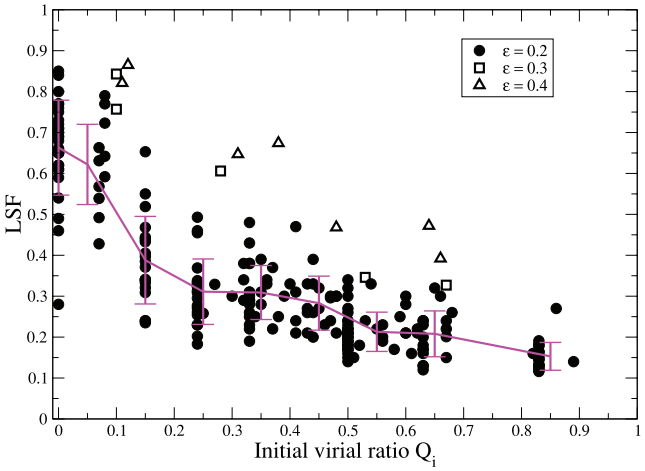

Figure 4. Plot of the initial virial ratio Q_i against the LSF at 3 Myr. Symbols reflect the initial true SFE of the region of 20, 30 or 40 per cent. Initially hot dynamical temperatures result in low LSF and conversely very cold dynamical temperatures result in high LSF. At a fixed value of the initial virial ratio, there is a slight trend for raised LSF for increasing true SFEs ϵ. Error bars show the mean and standard deviation of the scatter observed in the simulations with an initial true SFE of 20 per cent.

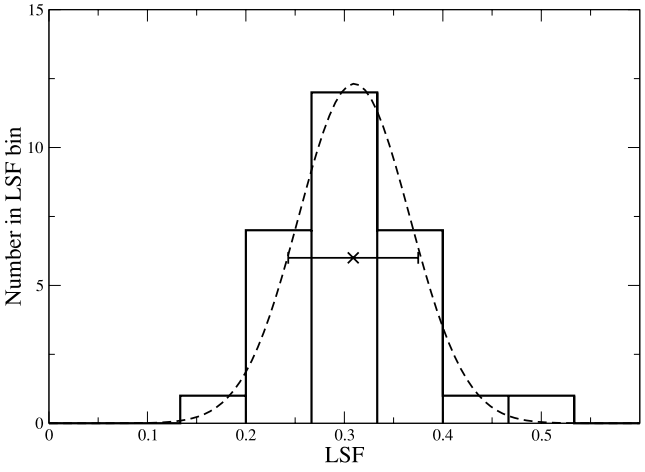

Figure 5. A representative histogram of the scatter in LSF within Q_i bin 0.1–0.2. Solid bars represent the numbers counted within each LSF bin. The cross point is the average LSF for all clusters within the bin. The error bars of the crossed point are the standard deviation of the LSF scatter. The dashed curve shows a Gaussian fit with equal standard deviation.

approximate equilibriums, and none of these clusters is fully virialized. We shall return to this point later.

3.2 Post-gas-expulsion evolution

After 3 Myr of evolution within the embedded phase (i.e. within the gas background potential), we assume that the gas is instantaneously expelled from the star-forming region. This is simply modelled by an instantaneous removal of the gas potential. We further evolve the gas-free star cluster an additional 3 Myr after gas expulsion. At this time, we measure the bound mass of the star cluster. Any star whose kinetic energy is less than its potential energy is considered bound. We normalize the bound mass by the total stellar mass in the simulation – this quantity is referred to as the *bound stellar fraction* ($f_{\rm bound}$).

In Fig. 7 we plot the bound stellar fraction $f_{\rm bound}$, as a function of the *initial* true SFE ϵ. We also plot the results of BK07 who used initial smooth and virialized equilibrium clusters as their initial conditions.

It is quite clear from this figure that our clusters with an initial true SFE of 20 or 30 per cent can survive gas expulsion with very significant fractions of their initial mass remaining. Also, there is a very significant scatter in our results rather than the very tight relationship found by BK07.

We confirm that our choice of 3 Myr of gas-free evolution has not significantly influenced our measured bound fraction by evolving a small sub-sample of clusters for 15 Myr after instantaneous gas removal. We continue the gas-free evolution phase of three clusters that result in a high-mass ($f_{\rm bound} = 0.72$), medium-mass ($f_{\rm bound} = 0.45$) and low-mass ($f_{\rm bound} = 0.30$) cluster when measured

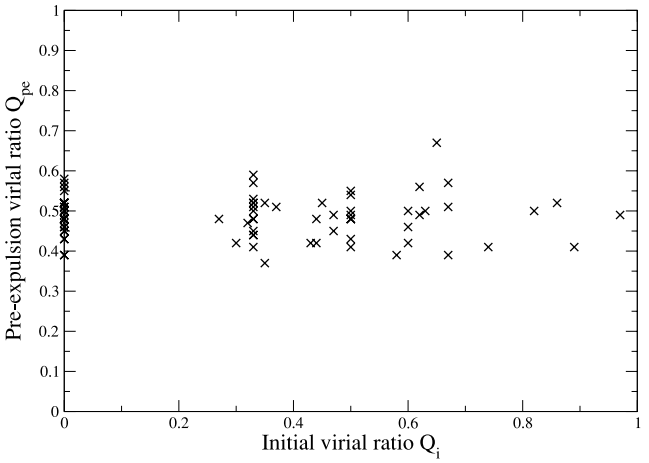

Figure 6. Comparison of the initial virial ratio Q_i, chosen at the beginning of the simulation, versus the pre-gas-expulsion virial ratio Q_{pe}, measured just prior to gas expulsion. Pre-expulsion virial ratios are all close to virialized ($Q_{pe} = 0.5$) but scatter around this value with a standard deviation of $\sim$0.05.

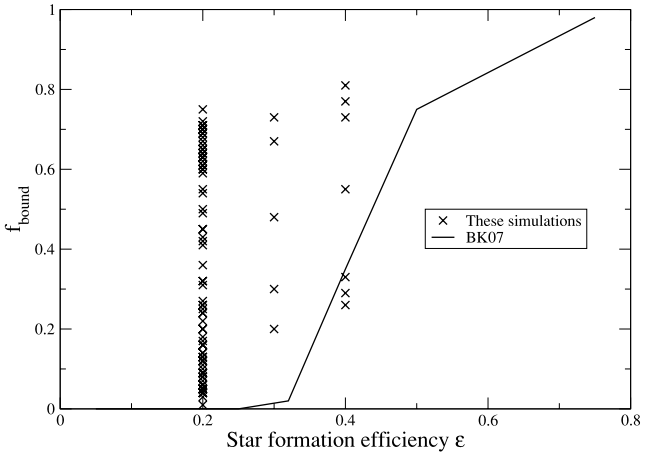

Figure 7. Plot of the region's SFE ϵ versus the final cluster's bound mass fraction f_{bound}. Crossed symbols are the results of all simulations in this paper whereas the solid line is the results of the BK07 simulations. The points are highly scattered with no clear trend and do not match the results seen in the BK07 simulations.

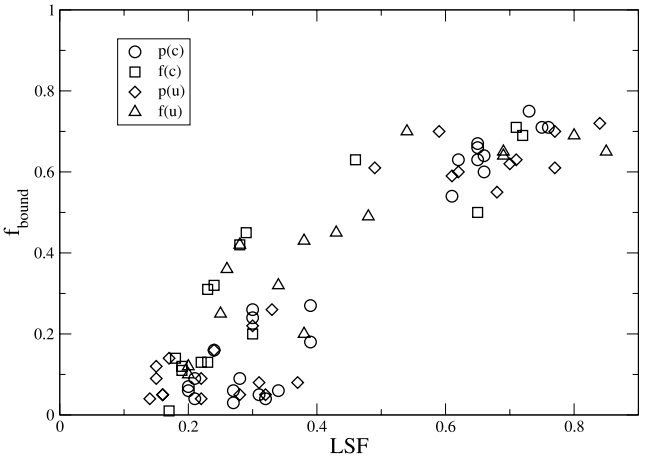

Figure 8. Plot of the influence of LSF (measured at the onset of gas expulsion) on the final bound mass fraction (f_{bound}) of clusters. All open symbols represent standard model simulations with varying initial stellar morphologies or gas potential concentrations. Key labels are fractal (f) or clumpy Plummer (p) morphology, and uniform (u) or concentrated (c) gas concentration. There is a good trend for increasing bound mass fraction with increasing LSF, although clearly there is scatter in the trend. The trend is independent of the initial stellar morphology or gas concentration.

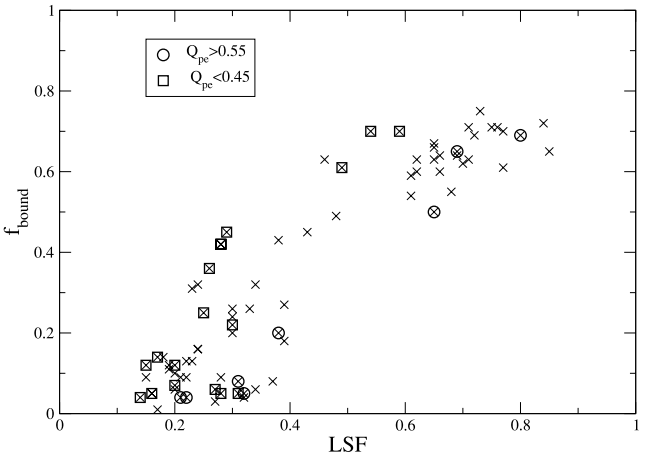

Figure 9. Plot of the influence of the dynamical state of the cluster (as measured by Q_{pe}) at the time of gas removal. All symbols in Fig. 8 (the standard model simulations) are now shown as crosses. Circle and square symbols represent simulations where $Q_{pe} > 0.55$ or $Q_{pe} < 0.45$, respectively, as indicated in the key.

after 3 Myr. After 15 Myr, the measured bound fraction differs by <5 per cent from those measured after 3 Myr.

The differences in our results from those of BK07 are in fact due to the differences in the initial conditions used for the simulations. As we have seen in the previous section, the effective SFE as measured by the LSF can increase significantly before gas expulsion. Rather than expecting a relationship with the initial SFE, we should expect a relationship with the LSF which we plot in Fig. 8. Here we find that the final bound fraction of stars does correlate with the LSF in a similar way to the results of BK07. Note that there is no systematic difference between the results of simulations of fractals or clumpy Plummers, nor with the concentration of the gas potential.

However, Fig. 8 shows that there is still a considerable scatter in the f_{bound}–LSF trend. Indeed, some clusters with an LSF of <0.3 can retain a significant bound fraction of stars after gas expulsion (up to 50 per cent). This is because the LSF is not the only parameter influencing stellar mass loss as a result of gas expulsion. The dynamical state of the cluster, as measured by Q_{pe}, is also expected to be important (Goodwin 2009). Recall from Fig. 6, by the onset of gas expulsion, that all clusters had become *approximately* virialized. However, even minor deviations from virial equilibrium at the onset of gas expulsion can significantly effect the cluster evolution post-gas-expulsion. In Fig. 9, we again plot the f_{bound}–LSF trend, but this time highlighting simulations whose pre-gas-expulsion virial ratio Q_{pe} is greater than 0.55 (super-virial) or less than 0.45 (sub-virial). Clusters that are slightly super-virial at the onset of gas expulsion clearly lie to the lower bounds of f_{bound}, whilst those which are sub-virial are at the higher end.

A gravitational system will reach approximate virial equilibrium in one to two crossing times, but it will tend to oscillate around exact virial equilibrium for some time (see also Goodwin 1997a). In

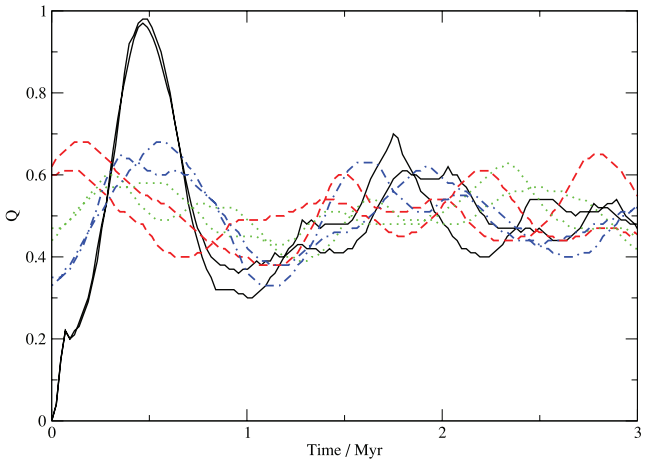

Figure 10. Time evolution of the virial ratio for $Q_{\rm i} = 0.0$ (solid, black lines), $Q_{\rm i} = 0.33$ (dot–dashed, blue lines), $Q_{\rm i} = 0.47$ (dotted, green lines) and $Q_{\rm i} = 0.6$ (dashed, red lines). The colour version is available online.

Fig. 10, we plot the evolution of the virial ratio with time during the embedded phase. We include representative curves for simulations with initial virial ratios of $Q_{\rm i} = 0.0, 0.33, 0.47$ and 0.6. All curves are results from simulations with a concentrated gas profile with a crossing time of 1.4 Myr. Whilst all clusters reach approximate virial equilibrium quite quickly, they oscillate around $Q = 0.5$ for some time. And, as shown in Fig. 9, the virial ratio they have at the moment of gas expulsion can make a significant difference to their ability to form a bound cluster afterwards.

4 DISCUSSION

We have shown that initially clumpy and out-of-equilibrium clusters will rapidly relax and erase most of their substructure. Depending on their initial virial ratios and substructure, this may mean that they may either collapse or expand. This will alter the importance of the gas potential on the stars meaning that initially cool clusters are more able to survive gas expulsion, whilst initially warm clusters are less likely to. This can reduce the dependency of survival to gas expulsion on the initial SFE, and place it instead on the initial dynamical state of the stars (see also Verschueren & David 1989; Goodwin 2009). We have also shown that there is a very significant scatter due to both the intrinsic differences between (statistically the same) clusters (see Allison et al. 2010) and the exact virial ratio at the onset of gas expulsion.

There is significant observational and theoretical evidence that the initial distributions of stars are not smooth nor are they virialized (see Elmegreen & Elmegreen 2001; Bate, Bonnell & Bromm 2003; Bonnell, Bate & Vine 2003; Bertout & Genova 2006; Allen et al. 2007; Kraus & Hillenbrand 2008; Gutermuth et al. 2009; Bressert et al. 2010; Clarke 2010, and references in all of these papers), which is a natural consequence of gravoturbulent star formation (see e.g. Elmegreen & Scalo 2004; Bergin & Tafalla 2007; McKee & Ostriker 2007; Clarke 2010). Indeed, evidence points towards sub-virial initial conditions for stars (see Allison et al. 2010, and references therein). We therefore argue that our initial conditions are far more realistic than those of a smooth, relaxed cluster as generally used before (e.g. Goodwin 1997a; Goodwin & Bastian 2006; BK07).

Proszkow & Adams (2009) conducted a large parameter study investigating the key parameters controlling the final bound fraction of clusters that have undergone gas expulsion using smooth and spherical initial stellar distributions. They found a clear trend with SFE although they, too, used sub-virial initial stellar distributions. We note that we also see a trend for increasing bound fraction with increasing SFE (Fig. 7), but that it is highly scattered. The source of this scatter is the use of clumpy initial stellar distribution. Therefore, the strength of the SFE as a predictor for the survival of a cluster to mass loss is severely weakened with the use of far more realistic initially clumpy stellar distributions.

It has often previously been assumed that for a cluster to survive, it must have had a high SFE and so the small numbers of clusters we see must be a high-SFE tail to the SFE distribution (see e.g. Parmentier et al. 2008). However, we have shown that some low-SFE clusters can survive if they are 'lucky' enough to have the right initial conditions. Indeed, the low survival rates found for young clusters of only ∼10 per cent (Lada & Lada 2003) may be better explained as these being the few clusters with the 'right' initial conditions than being an extremely high-SFE (>40 or 50 per cent) tail of star formation.

We note that our simulations are highly idealized. Stars are of equal mass, when Allison et al. (2009a) have demonstrated that rapid mass segregation can occur with a more realistic initial mass function.

We do not include any primordial binaries, although their presence can clearly influence the dynamics of a cluster (Goodman & Hut 1989). The simulations of Kroupa, Aarseth & Hurley (2001) show that changes in binary fraction and scattering between stars in the stellar outflow (that can result in binary hardening) can increase the final bound fraction of a cluster. In Moeckel & Bate (2010), the binary fraction does not change significantly during the cluster formation process as a result of formation in an initially high stellar density environment – within sub-clumps. However their initial conditions are limited to statistics of one, and we have further demonstrated that clumpy initial conditions can result in highly stochastic behaviour.

Furthermore we assume instantaneous gas removal, although BK07 demonstrated that a slower rate of gas removal can result in a higher cluster survival rate.

The length of the embedded phase is fixed at 3 Myr in our simulations although this could vary depending on the nature of the gas removal mechanism. Despite these simplifications, we argue that the idealized nature of the simulations has enabled us to more clearly test the implications of an initially sub-virial and clumpy stellar distribution. We defer a less idealized study to a later paper.

Our simulations do have an obvious problem, however, in that we use a smooth, static background potential for the gas. This has two main problems. First, the initial gas and stellar distribution do not match, despite the fact that our stars are assumed to have formed from this background gas. Secondly, the gas is not able to respond to the motion of the stars. (A third, but less important problem, is that we assume that all of the stars form instantaneously.)

The importance of both problems comes down to how well the motions of the gas and the stars are coupled. If conditions are such that both stars and (at least a significant fraction of the) gas move together in the potential, then we would expect both to collapse or expand together and the LSF and true SFE to remain roughly constant. However, if the bulk of the gas does not notice the stars because it is not involved in their formation and the relative gravitational influence of the stars is small, then our approximations should be roughly correct. We would argue that at low true star formation efficiencies, the bulk of the gas would be uncoupled from the stars. We are working on more detailed simulations with a live background potential which we will present in future papers.

5 SUMMARY AND CONCLUSIONS

We perform N-body simulations of substructured, non-equilibrium 500-$M_\odot$ clusters of $N = 1000$ equal-mass stars in a static background potential. The mass of gas is varied to simulate SFEs of 20–40 per cent. After 3 Myr of dynamical evolution, the potential is instantaneously removed to model the effect of gas expulsion from the cluster.

Previous work with initially smooth and equilibrium clusters has shown that there is a critical SFE for the survival of (at least part of) the cluster of ∼30 per cent (e.g. Goodwin & Bastian 2006; BK07, and references therein). However, it has also been known that it is the conditions *at the onset* of gas expulsion that are important in influencing the evolution of the star cluster following gas expulsion (Verschueren & David 1989; Goodwin 2009).

Our key results may be summarized as follows.

(i) The true SFE is not a good measure of the survival or otherwise of initially out-of-equilibrium clusters. Even though clusters rapidly come into approximate virial equilibrium, their structure can change significantly and, unless the gas follows the motions of the stars, the ratio of gas mass to stellar mass quantified by the LSF can change hugely.

(ii) It is the LSF, measured at the onset of gas expulsion, that is the key parameter controlling the survival of an embedded cluster to gas expulsion (see Fig. 8). A cluster with a high LSF at the onset of gas expulsion – regardless of the initial SFE – is able to produce a cluster with a significant fraction of the initial cluster mass after gas expulsion.

(iii) The dynamical state of the cluster, as measured by the virial ratio at the onset of gas expulsion, is also important. If gas expulsion occurs when the cluster is mildly sub-virial (i.e. collapsing), the cluster will suffer lower stellar mass loss as a result of gas expulsion. Conversely, a cluster that is mildly super-virial (i.e. expanding) at the onset of gas expulsion suffers greater stellar mass loss during gas expulsion.

The initial SFE of a cluster is almost certainly not a good measure of the ability of a cluster to survive gas expulsion. The initial spacial and kinematic distributions of the stars are crucial, as is how the stars and gas both evolve once the stars have formed. It is quite possible for low-SFE clusters (<20 per cent) to produce bound clusters after gas expulsion given the right initial conditions.

ACKNOWLEDGMENTS

MF was financed through FONDECYT grant 1095092, RS was financed through a combination of GEMINI-CONICYT fund 32080008 and a COMITE MIXTO grant and PA was financed through a CONCICYT PhD Scholarship.

REFERENCES

Aarseth S. J., 2001, MNRAS, 6, 277
Allen L. et al., 2007, Protostars and Planets V. Univ. Arizona Press, Tucson, AZ, p. 361
Allison R. J., Goodwin S. P., Parker R. J., de Grijs R., Portegies Zwart S. F., Kouwenhoven M. B. N., 2009a, ApJ, 700, L99
Allison R. J., Goodwin S. P., Parker R. J., Portegies Zwart S. F., de Grijs R., Kouwenhoven M. B. N., 2009b, MNRAS, 395, 1449
Allison R. J., Goodwin S. P., Parker R. J., Portegies Zwart S. F., de Grijs R., 2010, MNRAS, 407, 1098
Bastian N., Goodwin S. P., 2006, MNRAS, 369, L9
Bate M. R., Bonnell I. A., Bromm V., 2003, MNRAS, 339, 577
Baumgardt H., Kroupa P., 2007, MNRAS, 380, 1589 (BK07)
Bergin E. A., Tafalla M., 2007, ARA&A, 45, 339
Bertout C., Genova F., 2006, A&A, 460, 499
Boily C. M., Kroupa P., 2003a, MNRAS, 338, 665
Boily C. M., Kroupa P., 2003b, MNRAS, 338, 673
Bonnell I. A., Bate M. R., Vine S. G., 2003, MNRAS, 343, 413
Bressert E. et al., 2010, MNRAS, 409, L54
Chen H., Ko C., 2009, ApJ, 698, 1659
Clarke C., 2010, R. Soc. London Philos. Trans. Ser. A, 368, 733
Elmegreen B. G., 1983, MNRAS, 203, 1011
Elmegreen B. G., Clemens C., 1985, ApJ, 294, 523
Elmegreen B. G., Elmegreen D. M., 2001, AJ, 121, 1507
Elmegreen B. G., Scalo J., 2004, ARA&A, 42, 211
Geyer M. P., Burkert A., 2001, MNRAS, 323, 988
Goodman J., Hut P., 1989, Nat, 339, 40
Goodwin S. P., 1997a, MNRAS, 284, 785
Goodwin S. P., 1997b, MNRAS, 286, 669
Goodwin S. P., 2009, Ap&SS, 324, 259
Goodwin S. P., Bastian N., 2006, MNRAS, 373, 752
Goodwin S. P., Whitworth A. P., 2004, A&A, 413, 929
Gutermuth R. A., Megeath S. T., Myers P. C., Allen L. E., Pipher J. L., Fazio G. G., 2009, ApJS, 184, 18
Hills J. G., 1980, ApJ, 235, 986
Kraus A. L., Hillenbrand L. A., 2008, ApJ, 686, L111
Kroupa P., Aarseth S., Hurley J., 2001, MNRAS, 321, 699
Lada C. J., Lada E. A., 2003, ARA&A, 41, 57
Lada C. J., Margulis M., Dearborn D., 1984, ApJ, 285, 141
McKee C. F., Ostriker E. C., 2007, ARA&A, 45, 565
Mathieu R. D., 1983, ApJ, 267, L97
Moeckel N., Bate M. R., 2010, MNRAS, 404, 721
Parmentier G., Goodwin S. P., Kroupa P., Baumgardt H., 2008, ApJ, 678, 347
Pinto F., 1987, PASP, 99, 1161
Proszkow E., Adams F. C., 2009, ApJS, 185, 486
Tutukov A. V., 1978, A&A, 70, 57
Verschueren W., David M., 1989, A&A, 219, 105

This paper has been typeset from a TEX/LATEX file prepared by the author.